Available online at www.sciencedirect.com
ScienceDirect
Journal of Power Sources 172 (2007) 816–830
JOURNAL OF POWER SOURCES
www.elsevier.com/locate/jpowsour

One-dimensional thermal model of cold-start in a polymer electrolyte fuel cell stack

Manish Khandelwal [a], Sungho Lee [b], M.M. Mench [a,*]

[a] *Fuel Cell Dynamics and Diagnostics Laboratory, Department of Mechanical and Nuclear Engineering, The Pennsylvania State University, University Park, PA 16802, USA*
[b] *Research and Development Division, Hyundai Motor Company, Yongin 446-912, Republic of Korea*

Received 9 April 2007; accepted 7 May 2007
Available online 18 May 2007

Abstract

A transient, one-dimensional thermal model for a generic polymer electrolyte fuel cell (PEFC) stack is developed to investigate the cold-start ability and the corresponding energy requirement over different operating and ambient conditions. The model is constructed by applying the conservation of energy on each stack component and connecting the component's relevant boundaries to form a continuous thermal model. The phase change of ice and re-circulation of coolant flow are included in the analytical framework and their contribution to the stack thermal mass and temperature distribution of the components is also explored. A parametric study was conducted to determine the governing parameters, relative impact of the thermal mass of each stack component and ice, and anticipated temperature distribution in the stack at start-up for various operating conditions. Results indicate that 20 cells were sufficient to accurately experimentally and computationally simulate the full size stack behavior. It was observed that an optimum range of operating current density exists for a chosen stack design, in which rapid start-up of the stack from sub-zero condition can be achieved. Thermal isolation of the stack at the end plates is recommended to reduce the start-up time. Additionally, an end plate thickness exceeding a threshold value has no added effect on the stack cold-start ability. Effect of various internal and external heating mechanisms on the stack start-up were also investigated, and flow of heated coolant above 0 °C was found to be the most effective way to achieve the rapid start-up.

Keywords: Cold-start; Polymer electrolyte fuel cell; PEFC; Stack; Thermal model

1. Introduction

The current state of fuel cell technology faces a number of technical challenges for automotive application that must be surmounted in order to compete against the internal combustion engine. Among those, cold-start (i.e. start-up of polymer electrolyte fuel cell (PEFC) stack under freezing temperature) is a major bottleneck for achieving high performance and long-term durability [1–3]. In cold-weather conditions, the start-up of fuel cell stack is impeded by residual water ice formation, and water generated by electro-chemical reaction. The ice/frost formed may block the passage for reactant gas transport by filling the pores in the catalyst layer (CL) or diffusion media (DM), or block the channel flow path. To facilitate the rapid cold start-up process, energy is needed to melt the ice and heat up the fuel cell stack to its normal operating condition. Existence of phase change, and the various disparate length scales involved complicate the cold-start analysis. Detailed experimentation and modeling are needed to optimize both the stack design and the start-up protocol.

Currently, most of the existing stack models are concerned with the thermal and water management in the stack during steady state normal operating conditions [4–7]. Little information is available regarding the PEFC stack transient behavior and its performance under sub-zero conditions. Even though a significant number of system-based patents exists for cold-start e.g. [8–14], they fail to completely address the fundamental issues in the fuel cell stack during cold-start. Shan et al. [15,16] developed a transient stack system model to investigate the effect of varying load on the start-up during normal operating conditions.

* Corresponding author. Tel.: +1 814 865 0060; fax: +1 814 863 4848.
E-mail address: mmm124@psu.edu (M.M. Mench).

0378-7753/$ – see front matter © 2007 Elsevier B.V. All rights reserved.
doi:10.1016/j.jpowsour.2007.05.028

Nomenclature

A	cross-sectional area (m^2)
b	height of the stack (m)
C_p	specific heat ($J\,kg^{-1}\,K^{-1}$)
dm	mass of ice melted at current time step (kg)
F	Faraday's constant ($C\,mol^{-1}$)
h	convective heat transfer coefficient ($W\,m^{-2}\,K^{-1}$)
H	latent heat of fusion of water ($kJ\,kg^{-1}$)
i	current density ($A\,m^{-2}$)
k	thermal conductivity ($W\,m^{-1}\,K^{-1}$)
l	width of the stack (m)
$\dot{m}$	mass flow rate of reactant gases ($kg\,s^{-1}$)
n	number of electrons; number of coolant or gas channels
Q'''	volumetric heat source ($W\,m^{-3}$)
ΔS	change in entropy ($J\,mol^{-1}\,K^{-1}$)
t	thickness (m), time (sec)
T	temperature (K)

Subscript

amb	ambient air
bp	bi-polar plate
cp	coolant plate
CL	catalyst layer
DM	diffusion media
ep	end plate
g	gas channel
i	control volume
k	reactant/product gases
m	membrane

Latin symbol

η	over-potential (V)
ρ	density ($kg\,m^{-3}$)
σ	ionic conductivity ($S\,m^{-1}$)

Hishinuma et al. [17] evaluated the cold-start performance of a 104 cm^2 cell, both experimentally and numerically. They concluded that self-start-up of the given PEFC configuration below −5 °C was impossible without external heat input; although other stack design can self-start below −5 °C. Sundaresan and Moore [18] have presented a zero-dimensional thermal layered model to analyze the start-up behavior from a sub-zero environment. Their simulation incorporates the start-up transient, and captures the component level temperature distribution in the stack. However, their model is built on an identical empirical source term on the anode and cathode side, which prevents predicting the true asymmetric temperature distribution in the stack [15]. Moreover, each component in the stack is lumped and represented by a single point temperature, which limits the model to capture only the thermal mass effects rather than other material thermal parameters. Ahluwalia and co-workers [19,20] have investigated the effect of various operating conditions on the self-start of a PEFC stack using a two-dimensional species and current model. Details of various warming strategies including catalytic reaction [8,9], external load [10,11], passing hot fluid and reactant gas [12–14] in the PEFC stack, etc., have been developed and can be found in the published US patent literature. However, limited experimental data have been published so far due to the propriety nature of the field.

The current study is motivated by the need to provide useful guidelines to select the best stack materials and compare the various possible heating mechanisms for improving the PEFC stack cold-start performance. The objective of the present work is to develop a transient one-dimensional thermal model for a generic polymer electrolyte fuel cell (PEFC) stack to predict the temperature distribution, cold-start ability and energy requirement for the stack start-up under chosen operating and ambient conditions. Estimation of spatial temperature distribution and modeling of coolant/gas using convective heat transfer are the two distinct features of the model. Use of a convective heat transfer model for the gas/coolant flow eliminates the need of gas/coolant outlet temperature values, unlike other lumped models [4,18]. The motivation of this work is to examine the effects of thermal transport parameters, material and design variation of DM, the end plate and bi-polar plate, and external energy input on the sub-zero start-up of the PEFC stack, so that recommendations can be proposed to achieve rapid cold-start.

2. Model development

A typical PEFC stack consists of 200–250 single cells attached electrically in series. Each cell (consist of anode/cathode bi-polar plate, diffusion media (DM), catalyst layer and membrane) is separated by the coolant plate. The schematic of a typical PEFC stack is shown in Fig. 1.

2.1. Model assumptions

The following assumptions were made for the stack thermal model.

1. The heat transfer in the stack is one-dimensional (x-direction).
2. All material thermal properties are constant over the temperature range considered (−20 to 0 °C).
3. Thermal contact resistance between the PEFC components is neglected.
4. Joule heating is neglected in the DM, bi-polar plate and coolant plate due to the high conductivity and low start-up current density.
5. Reactant/product cross-over is not considered in the model, since it contributes negligibly to the heat generation.

2.2. Governing equation

The schematic of the stack and its components for the model development and control volume is shown in Fig. 2. In the current model, each stack component is resolved spatially in the x-direction, and conservation of energy is performed to

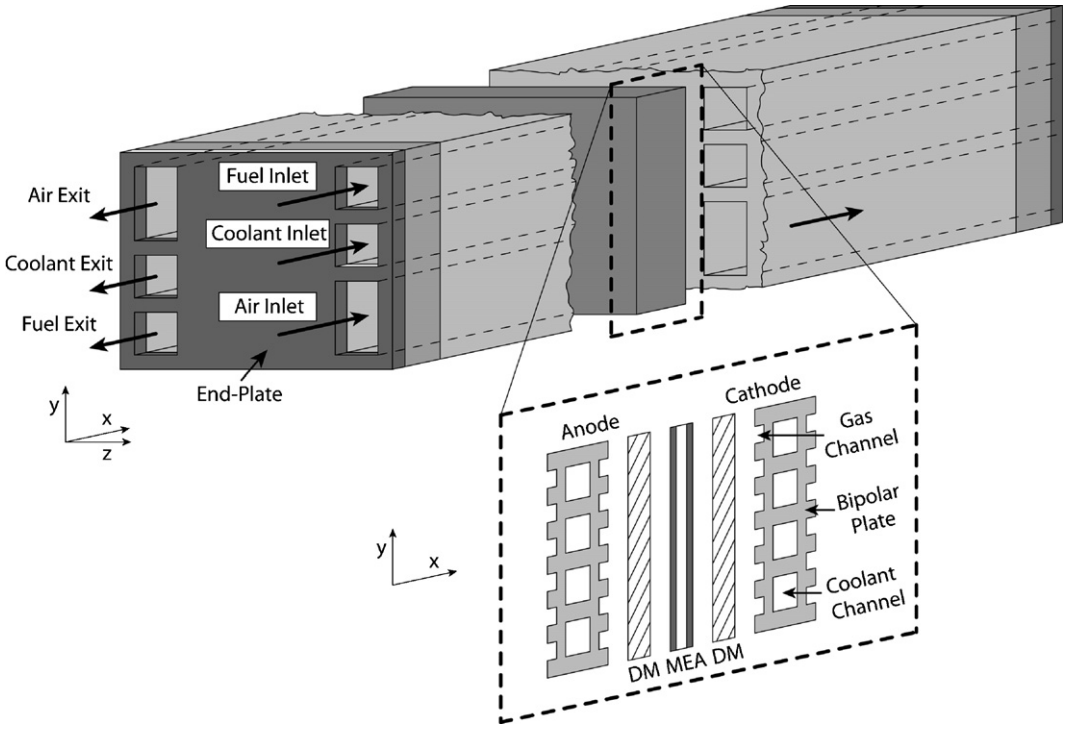

Fig. 1. Schematic of a polymer electrolyte fuel cell (PEFC) stack.

obtain the governing equation for the temperature. The detailed governing equation for each PEFC component is described below.

2.2.1. End plate

The end plate is normally made of polymer or metal and provides the uniform compression for the stack. Inside the end plate, conduction is the only mode of the heat transfer. One side of the end plate is exposed to the ambient or insulating material, and other side faces the coolant/current collector bus plate. Heat loss from the surface to the ambient air is treated as the flux boundary condition and is discussed in Section 2.3 in detail. The generalized governing equation for temperature [21] can be written as:

$$\frac{\partial T}{\partial t} = \left(\frac{k_{\mathrm{ep}}}{\rho_{\mathrm{ep}} C_{p,\mathrm{ep}}}\right) \frac{\partial^2 T}{\partial x^2} + \frac{Q'''_{\mathrm{ep}}}{\rho_{\mathrm{ep}} C_{p,\mathrm{ep}}} \tag{1}$$

The term on the left side is the rate of change of control volume temperature (i.e. thermal energy storage), the first term on the right side is the conduction heat transfer and the second term represents the volumetric rate of thermal energy generation in the control volume. The heat generation in the end plate during the normal operation is zero. However, for the cold-start, some additional external heating can be imposed as a warming strategy

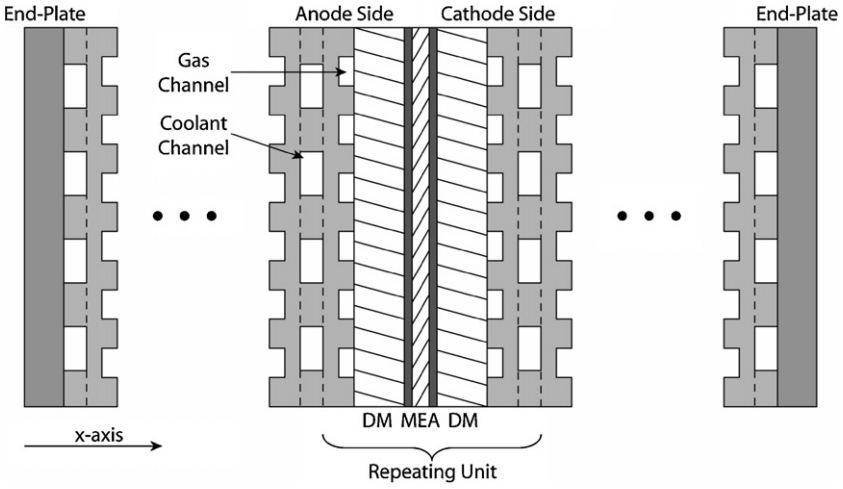

Fig. 2. Schematic of the PEFC stack and its components for one-dimensional model development.

to facilitate the rapid start-up. Therefore, the heat generation term is retained in the model formulation.

2.2.2. Coolant plate

In a fuel cell stack, cooling plates are used to remove the waste heat generated in the cell, and to maintain the designed stack temperature. The coolant plates are normally comprised of graphite/steel with machined or stamped flow channels. A detailed schematic for the coolant plate with various modes of relevant heat transfer is shown in Fig. 3a. The conduction heat transfer is considered through the solid part of the plate, whereas heat uptake from the stack body into the coolant is accounted through the convective mode of heat transfer (note that during start-up the *coolant* can actually heat or cool the stack depending on coolant and stack temperature). Moreover, the model can account for the time-dependent coolant inlet temperature during the start-up, enabling incorporation of the re-circulation of the coolant flow. Heat loss (convective and radiative) from the top and bottom of the coolant plate to the surrounding is accounted using an equivalent convective heat transfer coefficient (h_2). The governing equation in a coolant plate [21] can be written as:

$$\frac{\partial T}{\partial t} = \left(\frac{k_{\mathrm{cp}}}{\rho_{\mathrm{cp}} C_{p,\mathrm{cp}}}\right)\frac{\partial^2 T}{\partial x^2} - \left(\frac{1}{\rho_{\mathrm{cp}} C_{p,\mathrm{cp}}}\right)[2h_{\mathrm{cp}}(T - T_{\mathrm{coolant}}(t))n_{\mathrm{cp}} + 2h_2(T - T_{\mathrm{amb}})]\left(\frac{l}{A_{\mathrm{p}}}\right) + \frac{Q'''_{\mathrm{cp}}}{\rho_{\mathrm{cp}} C_{p,\mathrm{cp}}} \quad (2)$$

where n_{cp} is the number of coolant channels in the bi-polar plate, $T_{\mathrm{coolant}}(t)$ the time-dependent coolant inlet temperature, and A_{p} is the effective cross-sectional area available in the coolant plate for the conduction heat transfer. In Eq. (2), the first and second part of the second term on the right hand side represent the heat loss from stack to coolant and surrounding, respectively.

2.2.3. Anode/cathode bi-polar plate

In this formulation, the bi-polar plate is modeled similarly to the coolant plates, since these are typically a single integrated structure in a PEFC stack. The only difference in the bi-polar plate is that the gas channels are present in part of the plate, as shown in Fig. 3a. This structural difference is accounted in calculating the effective cross-sectional area for conduction heat transfer, A_{p}, which represent the total area of the lands in contact with the DM. The governing equation of bi-polar plate [21] can be written as:

$$\frac{\partial T}{\partial t} = \left(\frac{k_{\mathrm{bp}}}{\rho_{\mathrm{bp}} C_{p,\mathrm{bp}}}\right)\frac{\partial^2 T}{\partial x^2} - \left(\frac{1}{\rho_{\mathrm{bp}} C_{p,\mathrm{bp}}}\right)[2h_{\mathrm{g}}(T - T_{\mathrm{g}})n_{\mathrm{gc}} + 2h_2(T - T_{\mathrm{amb}})]\left(\frac{l}{A_{\mathrm{p}}}\right) + \frac{Q'''_{\mathrm{bp}}}{\rho_{\mathrm{bp}} C_{p,\mathrm{bp}}} \quad (3)$$

where n_{gc} is the number of gas channel in the bi-polar plate and T_{g} is the gas inlet temperature, and other parameters are defined in Nomenclature.

2.2.4. Anode/cathode diffusion media

The DM is an electrical conducting porous media located between the CL and the lands, and it provides a passage for the reactant gases to reach the reactant sites at the catalyst layer. In terms of heat transfer, the DM has the lowest thermal conductivity beside CL and membrane among the stack components [23], thus acting as insulation to the heat generating three-layer MEA structure. For the heat transfer model, the conduction heat trans-

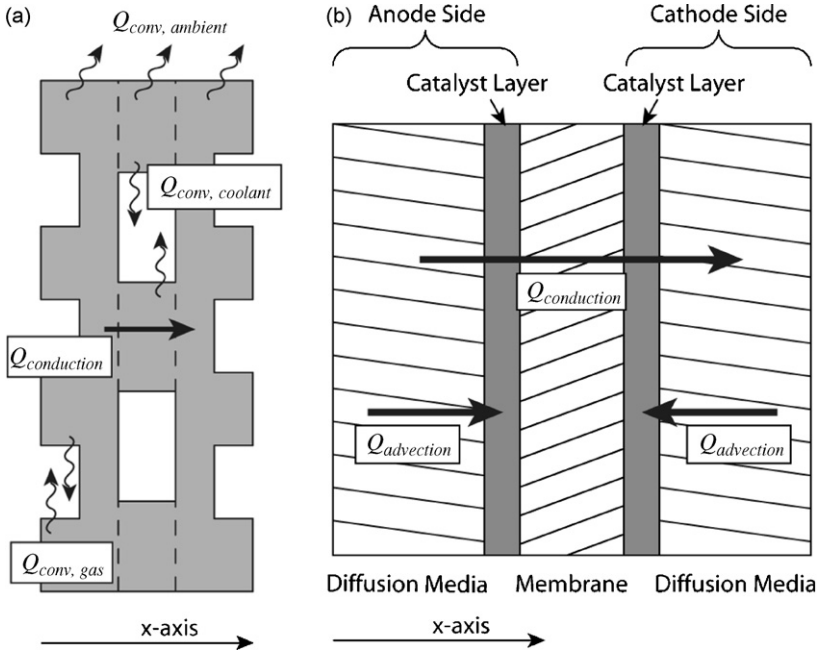

Fig. 3. Heat transfer mode in the PEFC stack component. (a) Bi-polar plate and coolant plate. (b) Diffusion media, catalyst layer and membrane.

fer through the bulk matrix and the advection heat transfer due to the reactant gas flow are considered to occur in the fibrous DM, as schematically shown in Fig. 3b. The heat generation in the DM occurs due to the ohmic heating of the carbon-based material. Due to the high ionic conductivity of DM, ohmic losses in the DM are negligible as compared to membrane and CL. So, no heat source in the DM is considered in the model. The governing equation can be written as:

$$\frac{\partial T}{\partial t} = \left(\frac{k_{\mathrm{DM}}}{\rho_{\mathrm{DM}} C_{p,\mathrm{DM}}}\right)\frac{\partial^2 T}{\partial x^2} - \frac{\sum \dot{m}_k \bar{C}_{p,k}}{A\rho_{\mathrm{DM}} C_{p,\mathrm{DM}}}\frac{\partial T}{\partial x} \tag{4}$$

The last term in Eq. (4) represents the advection heat transfer in the DM. The subscript k denotes the number of components of the reactant gas, including hydrogen, water–vapor and liquid water for the anode side DM and air, water–vapor and liquid water for the cathode side DM.

2.2.5. Anode/cathode catalyst layer

The CL is modeled similarly to the DM except for the addition of a heat generation term. The heat generation in the CL is due to the electro-chemical reaction and voltage over-potential. The volumetric heat source term in the CL can be written as:

$$Q'''_{\mathrm{CL}} = \frac{i}{t_{\mathrm{CL}}}\left(\frac{T_0\,\Delta S}{nF} + \eta\right) \tag{5}$$

where T_0 is the local catalyst temperature, and other parameters are defined in Nomenclature. The entropy change at standard state with platinum catalyst is taken as $\Delta S = 0.104\ \mathrm{J\,mol^{-1}\,K^{-1}}$ for the anode, and $\Delta S = -326.36\ \mathrm{J\,mol^{-1}\,K^{-1}}$ for the cathode [22]. The activation over-potential (η) was calculated based on typical Tafel kinetics for a Pt-electrode [33].

2.2.6. Membrane

The DuPont Nafion® or Gore Primea® membranes are widely used in fuel cell applications. In the membrane, conduction is the dominant mode of the heat transfer. The governing equation in the membrane can be written as:

$$\frac{\partial T}{\partial t} = \left(\frac{k_{\mathrm{m}}}{\rho_{\mathrm{m}} C_{p,\mathrm{m}}}\right)\frac{\partial^2 T}{\partial x^2} + \frac{Q'''_{\mathrm{m}}}{\rho_{\mathrm{m}} C_{p,\mathrm{m}}} \tag{6}$$

Note that the heat generation term in the membrane consists of Joule heating only.

2.3. Boundary/interface and initial condition

The left and right face of the end plates of the stack are exposed to the ambient air or insulating material. The convective flux boundary condition is specified as:

$$k\left.\frac{\partial T}{\partial x}\right|_{x=0} = h(T - T_{\mathrm{amb}}) \tag{7a}$$

$$-k\left.\frac{\partial T}{\partial x}\right|_{x=l} = h(T - T_{\mathrm{amb}}) \tag{7b}$$

where h is the convective heat transfer coefficient and can be calculated using natural convection correlations [21] or it can be assigned to a low value to simulate insulation conditions. At the interface of each stack component, the temperature and flux continuity are imposed. The initial condition in the model is presumed to be uniform with ambient temperature at all locations, which represents a fully soaked frozen stack. In a realistic scenario, days may be required to reach this uniform temperature condition. Therefore, this initial condition represents a worst-case scenario of start-up time and energy requirement.

2.4. Modeling of melting of ice and numerical implementation

The mathematical equations developed for each component were combined to form a single set of governing equation appropriate for all domains. These equations were discretized using the control volume method [24]. For the time discretization, the implicit technique was used. The required heat absorbed to melt the ice is modeled using the source-based method presented by Voller and Swaminathan [25] for the solidification process. The ice melts at 273 K and the temperature at that location (node) will not rise until all the ice melts. The generalized discretized equation for ith control volume can be simplified and written as:

$$A_i T_i^{n+1} + \sum_{\mathrm{nb}} B_{\mathrm{nb},i} T_{\mathrm{nb}}^{n+1} = D_i T_i^n - \left(Q_i''' - \frac{H(dm_i^{n+1})}{(A\,\Delta x)_i}\right)\Delta x_i + E_i \tag{8}$$

where A_i, $B_{\mathrm{nb},i}$, C_i, D_i and E_i are constant and depend on material properties and boundary conditions, T_{nb} the temperature of neighborhood control volumes, H the latent heat of fusion, Q_i''' and dm_i is the volumetric heat generation and the mass of ice melted at current time step in the ith control volume. Based on the available energy, the amount of initial ice melted is estimated using an iterative loop with Eq. (8). In the case of no initial ice, Eq. (8) is reduced in the discretized form of a transient diffusion equation [21]. The resulting set of discretized equations was solved using a tri-diagonal solver. Other details of numerical implementation can be found in ref. [26].

3. Stack parameter and verification

Based on the mathematical model described, a numerical code was developed to investigate the effect of various stack materials and operating parameters on the start-up behavior. Representative stack dimensions and other parameters for the base simulations are summarized in Table 1. For the base case, no coolant flow through the stack was considered and the initial ice content was assumed to be zero, representing a perfect purge shut down. Table 2 summarizes all necessary stack material thermal properties needed for the model. The convective heat transfer coefficients were estimated using the Churchill and Chu correlation [21] defined for natural convection. Well-established correlations for the fully developed flow were used for estimating the coolant and bi-polar plate channel convective heat transfer coefficient [21].

Table 1
Stack parameters for the base case simulation

Symbol	Parameter	Value
l	Width of the stack (m)	0.1 [18]
b	Height of the stack (m)	0.25 [18]
N	Number of cells	20
i	Current density in the stack (A m^{-2})	10,000 [18]
t_{ep}	End plate thickness (m)	0.025 [29]
t_{cp}	Coolant plate thickness (m)	0.001 [6]
b_{cp}	Coolant channel width (m)	0.005[a]
n_{cp}	Number of coolant channels in a single coolant plate	30[a]
t_{bp}	Bi-polar plate thickness (m)	0.001 [29]
b_g	Gas channel width (m)	0.001[a]
n_{gc}	Number of gas channels on the bi-polar plate	100[a]
t_{DM}	Anode/cathode DM thickness (μm)	400
t_{CL}	Anode/cathode CL thickness (μm)	25
t_m	Membrane thickness (μm)	50
T_{amb}	Ambient temperature (K)	253
T_g	Reactant gas inlet temperature (K)	253
T_{cp}	Coolant inlet temperature (K)	253
H	Latent heat of fusion of ice (kJ kg^{-1})	334 [21]

[a] Representative value is used.

Various test cases were designed and simulated to rigorously verify the developed numerical code. Details of the verification, grid and time sensitivity studies are shown in ref. [26]. From the grid sensitivity study, it was concluded that 140 grid points per cell were sufficient to ensure the spatial error to be less than 0.04%. Similarly, time step sensitivity study results in less than 0.02% error with time step of 0.1 s for simulations without initial ice, whereas time step of 0.01 s is needed to achieve the same level of accuracy for a case with initial ice.

The key definitions used to describe the results are described below:

Start-up time (s): Start-up time is defined here as the time to reach the assured self-start-up condition. That is, *when the temperature at each node in stack* (*except the end plate*) *is greater than* 0 °C, *and all the ice in the stack has been melted*. Note that, depending on the design, a stack may achieve operational start-up before this condition is strictly achieved. However, it serves as a natural baseline for the comparison.

Normalized energy generation (J m^{-2}): Normalized energy generation is defined as $Q_{gen}/(N_{cell} \times$ active area of the stack), where Q_{gen} is the total heat energy generated in the stack (including external heat source). This parameter can be used to compare different size PEFC stacks during start-up.

4. Results and discussion

Results are presented for the baseline parameters and the start-up condition shown in Table 1, unless otherwise specified. For computational efficiency, a sensitivity study of the number of cells on start-up time and normalized energy was performed and is shown in Fig. 4a. The purpose of this was to determine the minimum number of cells needed to realistically predict the behavior of a full size stack with 200–250 cells. Moreover, this is also an important factor in the cold-start experimental design. For experimental convenience, the number of cells in the stack should be minimized. At the same time, the short stack should accurately predict the full size stack start-up behavior. Therefore, a general criterion to assure computational and experimental accuracy with a short stack is needed. Based on the baseline parameters in Table 1, it was found that a stack with 20 cells or more was sufficient to accurately simulate full size stack thermal behavior. To further investigate the appropriateness of the chosen minimum number of cell (20 cells), the temperature distribution for 10, 20 and 30 cell stack were computed and compared in Fig. 4b. The temperature distribution in the center cells for 20 and 30 cell stack were almost identical; indicating that 20 cell stack analysis is adequate to extrapolate the full size stack temperature distribution and start-up behavior. Recognizing the fact that minimum number of cell is a strong function of end plate and stack component design, the results presented here are applicable to the baseline conditions chosen for the generic stack, and will not be valid for all stack configurations. As stack configura-

Table 2
Thermal/material properties of the stack components

	Material	Thermal conductivity, k (W m^{-1} K^{-1})	Density, ρ (kg m^{-3})	Specific heat, C_p (J kg^{-1} K^{-1})	Ionic conductivity σ (S m^{-1})
End plate	Polymer [29]	0.32 [29]	1740 [21]	1460 [21]	Insulator
Coolant plate	Graphite [6]	10 [21]	1400 [21]	935 [21]	–
Anode bi-polar plate	Graphite [29]	10 [21]	1400 [21]	935 [21]	–
Diffusion media	Carbon paper	0.42 [23]	450 [30]	710 [21]	1250 [30]
Catalyst layer	–	0.27 [23]	1000[a]	710 [21]	2.4, 30% ionomer
Membrane	Nafion	0.16 [23]	1980 [31]	1170[b]	8 [32]
H_2 (at 270 K)	–	0.165 [21]	0.090 [21]	14,160 [21]	–
Air (at 270 K)	–	0.0223 [21]	1.30 [21]	1005 [21]	–
	Plain carbon steel	60 [21]	7850 [21]	430 [21]	
	Stainless steel	13.4 [21]	8238 [21]	935 [21]	

[a] Calculated as catalyst mixture property based on typical mixture fraction of carbon, Pt and ionomer.
[b] Same as polytetrafluoroethylene (PTFE).

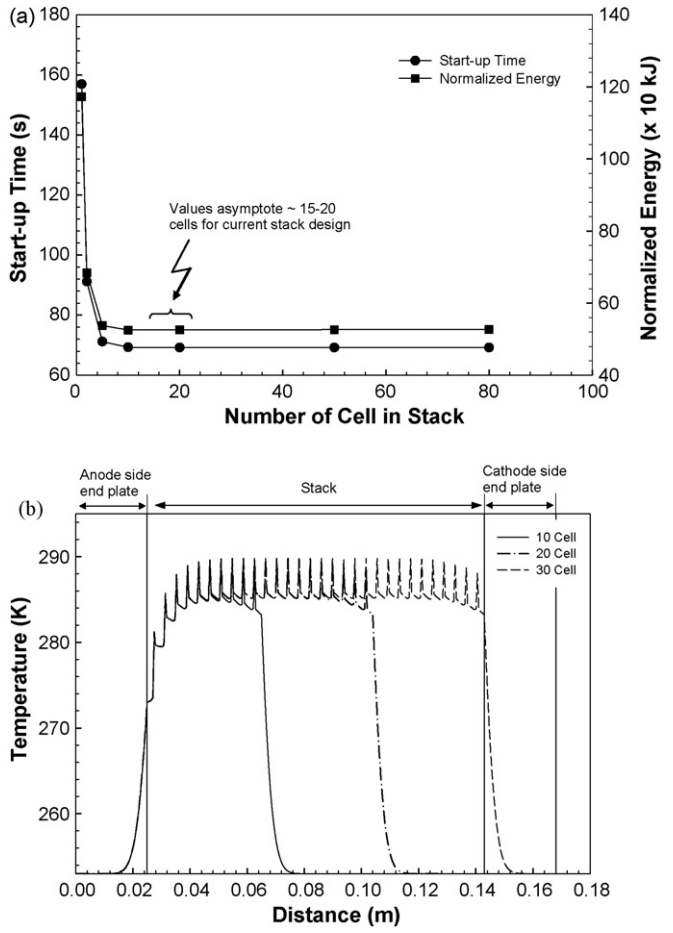

Fig. 4. (a) Variation of start-up time and normalized energy generation with the number of cells, initial temperature = −20 °C and base conditions. (b) Temperature distribution at the end of start-up (t = 69.2 s) for 10, 20 and 30 cell stack.

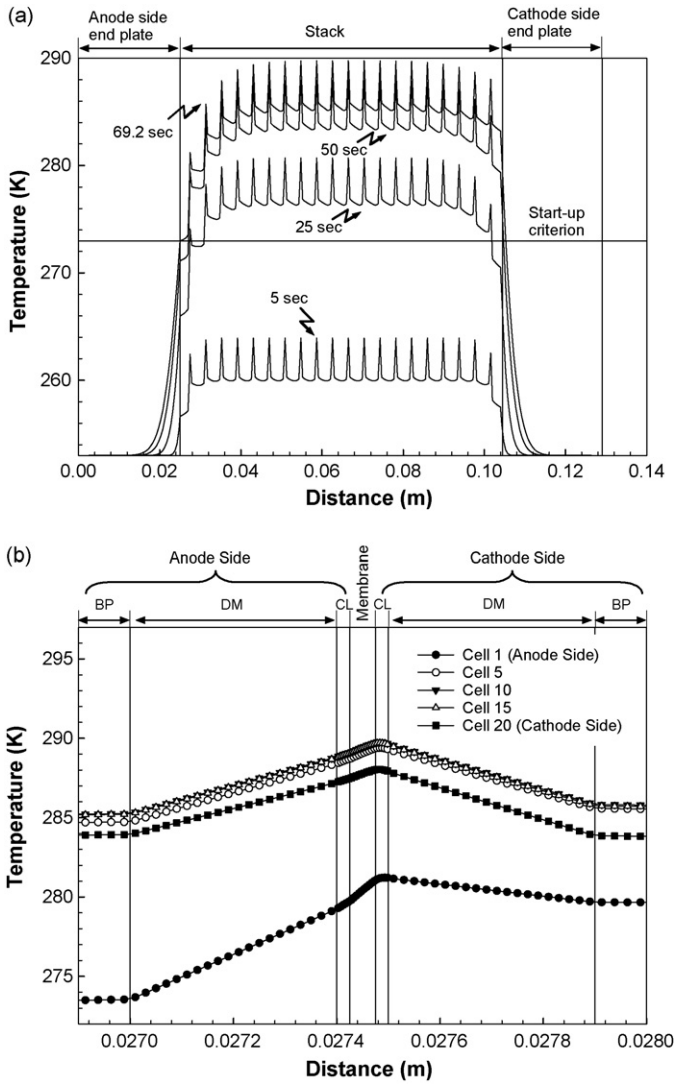

Fig. 5. (a) Stack temperature profile for base conditions at various time for i = 1.0 A cm^{-2} (start-up time = 69.2 s), T_{amb} = −20 °C without ice and no coolant flow. (b) Cell temperature profile at t = 69.2 s.

tions become optimized with lower thermal mass, the minimum cell requirement will decrease.

4.1. Variation of operating current density

Figs. 5a and 6a show the stack temperature profile during the start-up from −20 °C for current densities i = 1.0 and 0.1 A cm^{-2}, respectively. At higher current density (i = 1.0 A cm^{-2}) without any coolant flow and zero initial ice, the start-up condition was achieved in 69.2 s (Fig. 5a). However, the start-up condition was not reached for i = 0.1 A cm^{-2} and is shown in Fig. 6a. For this case, the heat losses from stack to the reactant gases and the ambient air (both at −20 °C) could match the heat generation, thus preventing the stack from reaching a temperature above 0 °C. The asymmetric stack temperature distribution of Fig. 5a can be attributed to the different heat source term on the anode and cathode side. Similar trends for stack temperature distribution are also observed by Shan and Choe [15]. The higher heat generation at 1.0 A cm^{-2} is the key factor for the rapid start-up as compared to the lower current density (i = 0.1 A cm^{-2}). *Note that in these simulations, freeze-out blockage and shut down from ice generated by electro-chemical reaction are not considered, and these results are intended for thermal comparison only*. There is also a balance between water generated freeze-out and heat generation that results in an optimal current density. In Fig. 6a, the stack temperature distribution reaches steady state beyond 100 s. At i = 0.1 A cm^{-2}, all the generated heat is transferred to the reactant gas or ambient air, or used in increasing the end plate sensible energy (i.e. temperature), to reach the steady state condition. Self-heating of the stack to above 0 °C is impossible, if the stack reaches such an equilibrium condition. Therefore, all the heat losses must be minimized to achieve the rapid start-up. Heat loss to the reactant gas or coolant can be reduced either by increasing the inlet gas flow temperature or reduction in the gas flow rate. The effect of inlet gas temperature and end plate effect is analyzed in the next section.

Figs. 5b and 6b show the temperature distribution of center and end cells at the end of start-up for current densities i = 1.0 and 0.1 A cm^{-2}, respectively. For i = 1.0 A cm^{-2}, the center cells

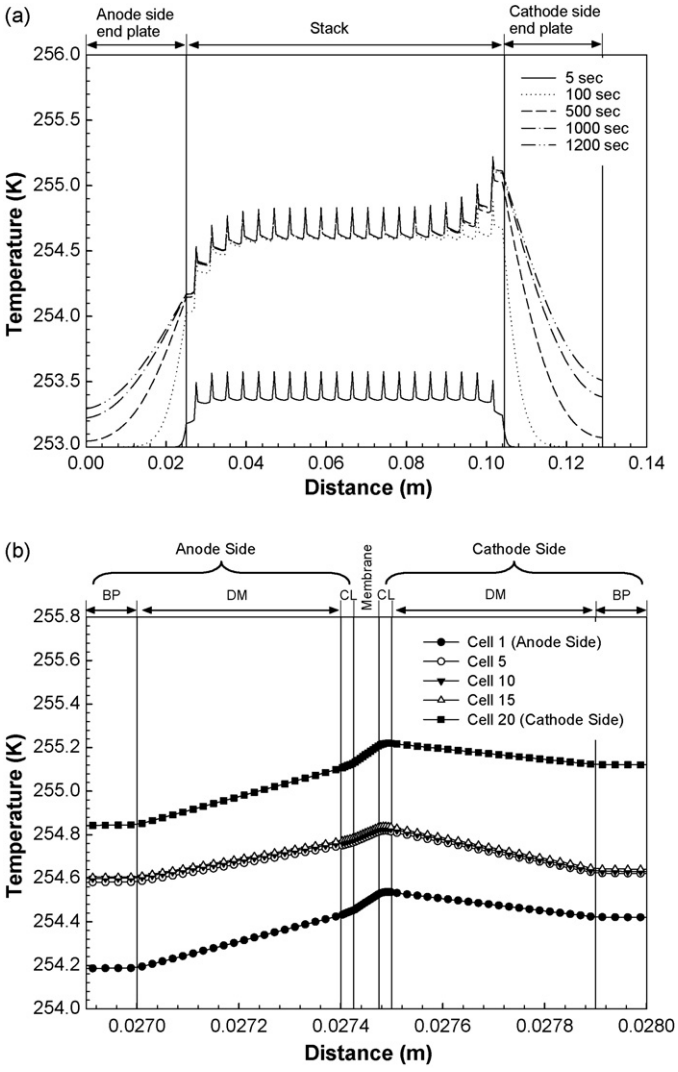

Fig. 6. (a) Stack temperature profile for base conditions at various time for $i = 0.1\ \mathrm{A\,cm^{-2}}$ (no start-up to 1200 s), $T_{amb} = -20\ ^{\circ}\mathrm{C}$ without ice and no coolant flow. (b) Cell temperature profile at $t = 1200$ s.

have the maximum temperature and can be 20–25 °C higher than the anode side end cell (cell 1) during the start-up. The cathode side end cell (cell 20) was 2–3 °C lower than maximum stack temperature. However, for $i = 0.1\ \mathrm{A\,cm^{-2}}$, a temperature gradient was formed in the stack, with the highest temperature on the cathode side end cell (cell 20) and the lowest on the anode side end cell (cell 1). Interestingly, this temperature gradient is a result of asymmetric heat source in the cell coupled with the higher convective heat loss on the anode side gas channel. For the baseline channel design and the flow rate, the reactant flow on both sides is laminar ($Re_{anode} \sim 50$, $Re_{cathode} \sim 600$). The higher convective heat transfer coefficient on the anode side is due to the significantly higher (approximately seven times) thermal conductivity of hydrogen gas as compared with air, as shown in Table 2.

The convective heat transfer coefficient (h) in the reactant gas channels depends on the channel design and dimension, the flow rate, and the species mixture. At higher current densities ($\sim 1\ \mathrm{A\,cm^{-2}}$), higher flow rate increases h, thus increasing the convective heat loss to the incoming flow at −20 °C. However, higher current density operation is also accompanied with higher heat generation, which may overcome the additional heat losses from the stack. Therefore, an appropriate thermal based threshold operating current density can be defined for the self-start of the PEFC stack where heat generation is greater than reactant and external heat loss. At higher current density operation, more water is also generated, which may freeze at the catalyst layer and potentially lead to the shutdown of the cell/stack. So, there is also an appropriate water generation based operating current density for the cell/stack during the cold-start, which is difficult to estimate. It can be concluded that there exists an optimal current density for a given design that balances heat generation with freeze-out from the water generated from reaction. Hishinuma et al. [17], Ahluwalia and Wang [19] have also reported similar observation for the critical/optimal voltage and operating current density during the cold-start of a unit cell and stack, respectively. A coupled heat and mass transfer model with detailed current and species conservation is necessary to quantitatively estimate this optimum range of operating current density, however it is out of the scope of this paper.

Fig. 7 shows a pie-chart for the sensible energy flow in each stack component estimated by a lumped model presented in literature [18] and the current one-dimensional thermal model. The sensible energy is normalized for the direct comparison between both the models, and the presented results are for base case condition with $10\ \mathrm{mg\,cm^{-2}}$ initial ice distribution (refer to Table 3).

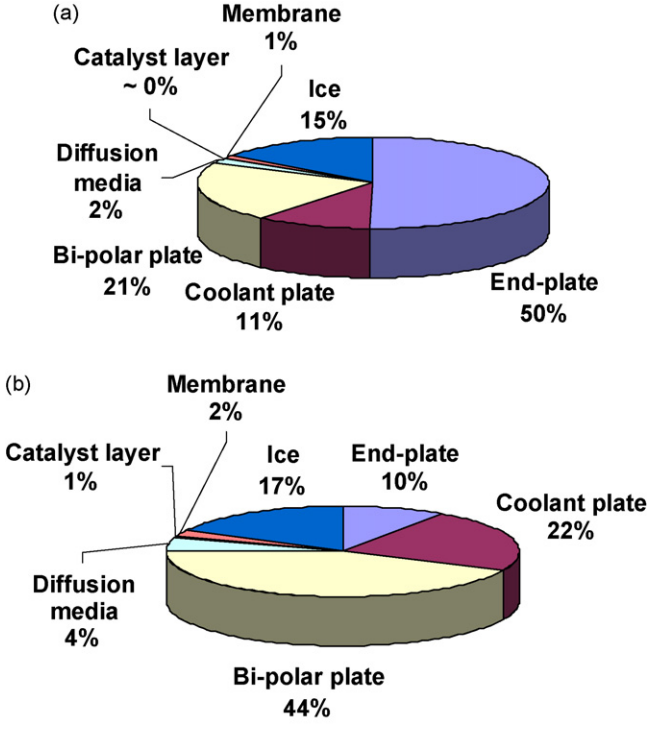

Fig. 7. Relative percentage distribution of normalized sensible energy at the component level for 20 cell stack, needed to achieve start-up condition from −20 °C with $10\ \mathrm{mg\,cm^{-2}}$ ice per cell (a) lumped model; (b) one-dimensional thermal model.

Table 3
Effect of initial ice distribution on the start-up time for 250 cm^2 active area stack and $i = 1\ A\ cm^{-2}$ (cell components thickness are for base condition)

Amount of ice per unit active area (mg cm^{-2})	Ice distribution in each component of a single cell (mg)			Start-up time (s)	% Increase in start-up time
	DM	CL	Membrane		
0	0	0	0	69.09	–
1	160	40	50	70.23	1.65
2	320	80	100	71.41	3.36
3	480	120	150	72.62	5.11
5	800	200	250	75.13	8.74
7	1120	280	350	77.47	12.13
10	1600	400	500	81.82	18.43
0.4	100	0	0	69.59	0.72
0.4	0	100	0	69.45	0.52
0.4	0	0	100	69.44	0.51

The 10 mg cm^{-2} of ice is presumed based on the estimate of residual stored water content from extensive Neutron Imaging studies at the Pennsylvania State University with conventional DM materials [27]. The lumped model estimates a substantially higher amount of sensible energy is invested in the end plate (∼50%) compared to the current one-dimensional model (∼10%). In the one-dimensional model, the bi-polar and coolant plates dominate the sensible energy requirement (∼70%) among the other stack components. This analysis indicates that bi-polar and coolant plate thermal mass are the key factors for the cold-start, rather than the end plate thermal mass as discussed by others [18]. In fact, one clear objective to rapid start is reduction of the energy stored in the end plates, as it does nothing to aide start-up. It was also observed that the relative energy distribution between components depends on the stack design, and will change as the stack design improvements are made. For example, as bi-polar plates are made thinner in the future, the overall contribution for the soft goods (i.e. MEA and DMs) will become critical. Even though this is not the case with the baseline bulky bi-polar and end plates of the present study. With the baseline stack design, 15–20% of the energy during the start-up is also spent to melt the initial ice, indicating the strong role of purging of residual water in reducing the start-up time and energy required. Detailed analysis of end plate and bi-polar plate thermal parameters, and impact of initial ice are presented in the subsequent sections.

4.2. Effect of the inlet gas temperature

The effect of inlet gas temperature on the stack start-up time for $i = 1.0\ A\ cm^{-2}$ is shown in Fig. 8. This plot shows a significant reduction in the start-up time with an increase in the anode gas inlet temperature. The start-up time decreases from the 69 s to less than 20 s with heated gas flow above 0 °C. The cathode side heating however is not effective. For anode or cathode side heating only, the inlet temperature of the non-heated inlet gas was maintained at 253 K (−20 °C). Similar enhancement of cold-start ability is experimentally observed by Yan et al. [28] for the single cell. Heating the anode side is much more effective than the cathode side due to the high heat transfer coefficient for hydrogen compared to air, as discussed earlier. Considering the low relative flow rate and thermal dominance of the anode side, the additional external heating required to raise anode gas temperature greater than 0 °C may be worthwhile in some system designs. Although to achieve this, the center manifold would need to be also heated. Heating the anode gas has the added benefit of reducing the temperature difference between the anode and cathode side that naturally arises due to the unbalanced heat generation in the electrodes. Cathode flow heating may not be useful from a thermal perspective, although enhanced product water uptake can be useful in terms of effective mass transport and retarding the freeze-out.

4.3. Effect of the initial ice distribution

Residual water may freeze inside the fuel cell and drastically change the stack cold-start ability and the energy requirement. Table 3 summarizes the start-up time (ambient temperature −20 °C) for different initial ice distributions in the fuel cell stack components. The total amount of initial ice was distributed proportionally in the DM, the CL and the membrane, and is also shown in Table 3. For the baseline stack design, the start-up time increases almost 18% with increasing the initial ice from 0 to 10 mg cm^{-2} per cell. In practice, the fuel cell may be frozen out before achieving the start-up criteria due to the block-

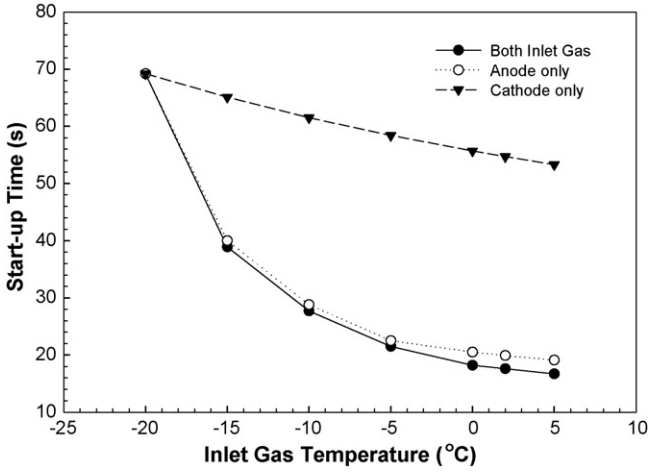

Fig. 8. Effect of inlet reactant gas temperature on the start-up time.

age of reactant gas in the CL (refer to Section 4.1 for details). The relative sensible energy requirement for each stack component with 10 mg cm^{-2} ice per cell is also shown in Fig. 7b. The one-dimensional thermal model predicted that almost 17% of the total sensible energy is used to melt the ice for case of 10 mg cm^{-2} ice per cell, indicating the importance of proper drainage and purge on shutdown. With the advancement in the stack design, the fraction of sensible energy required for the ice and soft goods can increase to very high percentage (>50%), emphasizing the need of an optimized purging method, selection of DM and channel design that naturally carry low liquid content during regular operation. Moreover, the effect of ice is more critical at lower current density ($i < 0.1$ A cm^{-2}), due to the lower heat generation. In such scenarios, external pre-heating of the stack before its operation may be needed to mitigate the ice effect and reduce the start-up time.

4.4. Effect of the bi-polar/coolant plate

The variation of thermal parameters of the bi-polar/coolant plate material and simulation results for some standard bi-polar plate materials are shown in Fig. 9. Fig. 9a shows the variation of start-up time with thermal conductivity of the bi-polar/coolant plate material for different specific heats. Two extreme cases for the specific heat, $C_p = 200$ and 2000 J kg^{-1} K^{-1} are shown in Fig. 9a. It is obvious that reducing the thermal mass will significantly decrease the stack start-up time. However, the start-up time is found to be invariant for plate thermal conductivity higher than 10 W m^{-1} K^{-1}. This can be attributed to the lower thermal conductivity (~20–25 times) of the soft goods, including DM, CL and membrane [23]. The bi-polar plates appear to behave as a pure heat conductor, thus negligible change in the start-up time was observed with change in $k_{BP} > 10$ W m^{-1} K^{-1}. Given that $k_{BP} > 10$ W m^{-1} K^{-1} in almost all possible bi-polar plate materials, the most important characteristic of the bi-polar plate is the specific heat and size. Fig. 9b shows a bar-chart for the energy requirement and start-up time for various bi-polar/coolant materials. Even though for the same geometry and dimension, metallic bi-polar plates are much worse than the graphite due to higher specific heat, the use of thinner stainless steel plate (half thickness of the base case) reduces the start-up time by 40% as compared to the thicker graphite plate (base case). Considering that reduced thickness of metal bi-polar plates can be much greater than the simulated case (half thickness), metallic plates offer a significant decrease in start-up time compared to graphite bi-polar plates. With this improvement however, the residual ice content and soft goods become increasingly significant. In summary, materials having thermal conductivity greater than 10 W m^{-1} K^{-1} with minimum thermal mass are recommended for the bi-polar/coolant plate.

4.5. Effect of the end plate

Fig. 10 shows the effect of the end plate thermal parameters on the start-up time and results for some standard end plate materials. The variation of start-up times with the end plate ther-

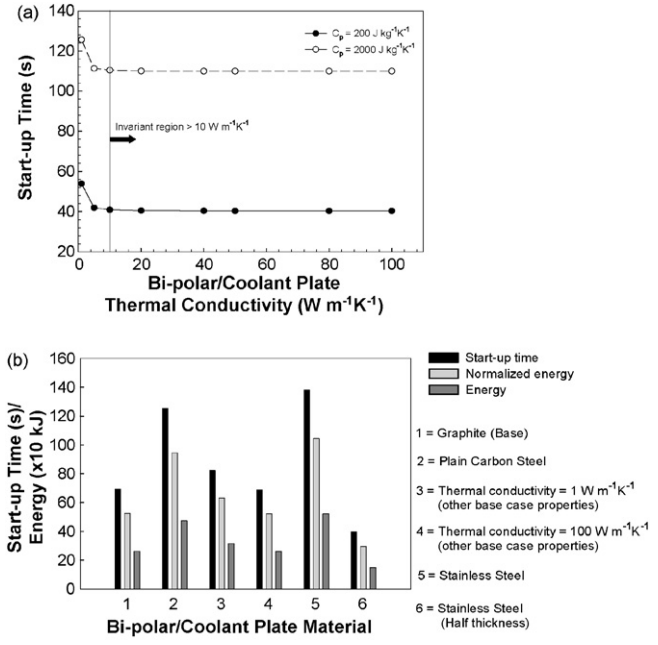

Fig. 9. (a) Effect of bi-polar/coolant plate thermal conductivity on the start-up time for different specific heat ($\rho = 1400$ kg m^{-3}, $C_p = 200$ and 2000 J kg^{-1} K^{-1}). (b) Start-up time and energy generation for various standard bi-polar plate materials.

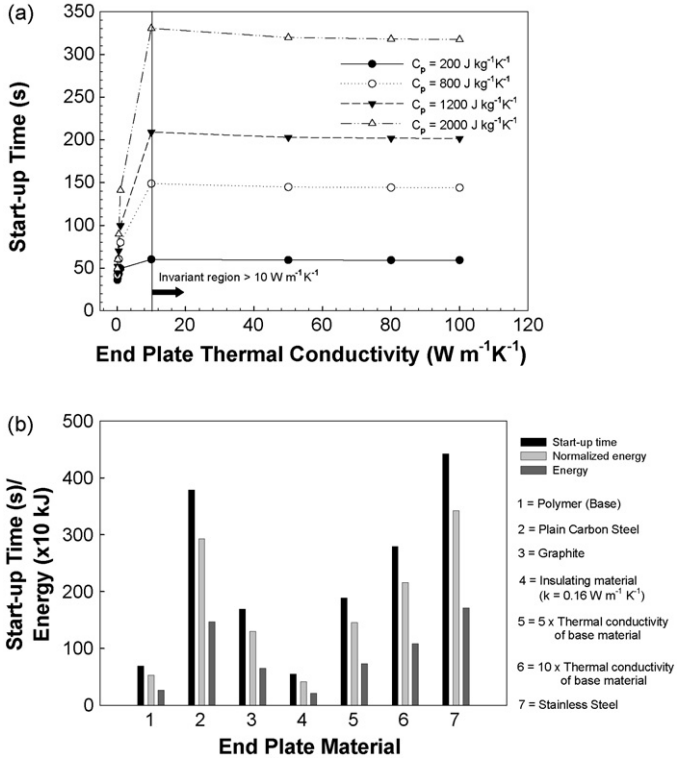

Fig. 10. (a) Effect of end plate thermal conductivity on the start-up time for different specific heat ($\rho = 1400$ kg m^{-3}, $C_p = 200$, 800, 1200 and 2000 J kg^{-1} K^{-1}). (b) Start-up time and energy generation for various standard end plate materials.

mal conductivity, for different specific heat values is shown in Fig. 10a. With an increase in the end plate thermal conductivity, the start-up time increases and reaches an asymptotic value around a plate thermal conductivity value of $10\,W\,m^{-1}\,K^{-1}$. This increase in the start-up time is due to the poor thermal insulation (thermal conductivity $> 10\,W\,m^{-1}\,K^{-1}$) provided by the end plate. However, with an increase in the specific heat (or ρC_p), the start-up time increases almost linearly. From Fig. 10b, the start-up time for metallic end plates (like stainless or plain carbon steel) is four to five times higher than the base case, and may not be suitable for rapid cold-start. However, use of an insulating material like polymers with good mechanical strength is a better option for the end plate. If the metallic plates are chosen for the end plate, thermal isolation by an additional insulation layer between the stack and current collector plate would improve the cold-start ability of the stack. A key during start-up is to minimize the total heat transfer to the end plates, since the end plate simply acts as a heat sink during the start-up.

The effect of the end plate thickness on the start-up time is shown in Fig. 11. It can be easily observed that increasing the end plate thickness first increases the start-up time drastically (due to the increase in thermal mass) until reaching a constant value. For the base conditions, an end plate thickness greater than 10–15 mm has no further effect on the start-up time or the total energy requirement. The reason for this behavior is that the start-up condition has been achieved before the thermal waves propagate through the thicker end plate. If one considers a case of infinite end plate thickness, this behavior is more easily understood. To examine this observation, the temperature distribution for different end plate thickness is shown in Fig. 11b using a normalized scale. The right hand side ($x = 1$) of the plot is towards the stack and the left side ($x = 0$) is facing to the ambient air. For thicknesses of 10, 25 and 45 mm, the temperature in the end plate towards the ambient side is still 253 K (initial condition), and temperature change can be observed in 20–60% of the end plate only. So, increasing the thickness has no effect on the temperature distribution beyond a certain value, and thus the start-up time and required energy remains same. Knowledge of this threshold end plate thickness (which is again a function of design and start-up conditions) can be very helpful for the stack design. If stack design requires an end plate thickness higher then its threshold value to satisfy compression requirement, then the plate thickness can be increased without affecting the stack cold-start behavior. As discussed, however, thermal isolation between the end plate and current collector/coolant plate is preferred.

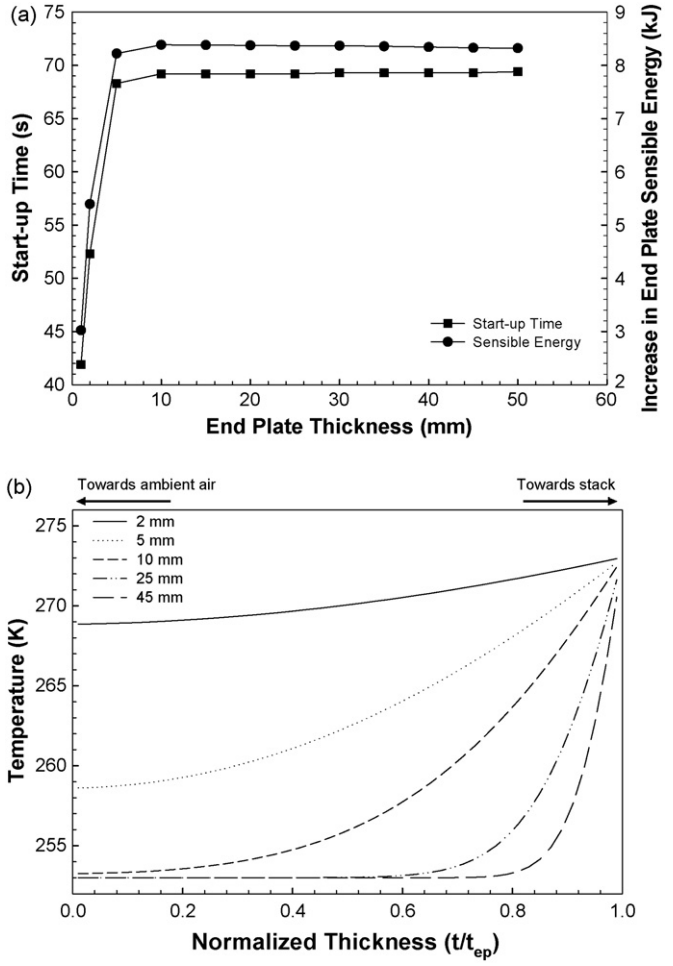

Fig. 11. (a) Effect of end plate thickness on the start-up time and increase in the end plate sensible energy during the start-up. (b) Temperature distribution in the end plate on a normalized thickness dimension.

4.6. Effect of diffusion media

The effect of diffusion media thermal conductivity on the start-up time and results for various commercially available DM

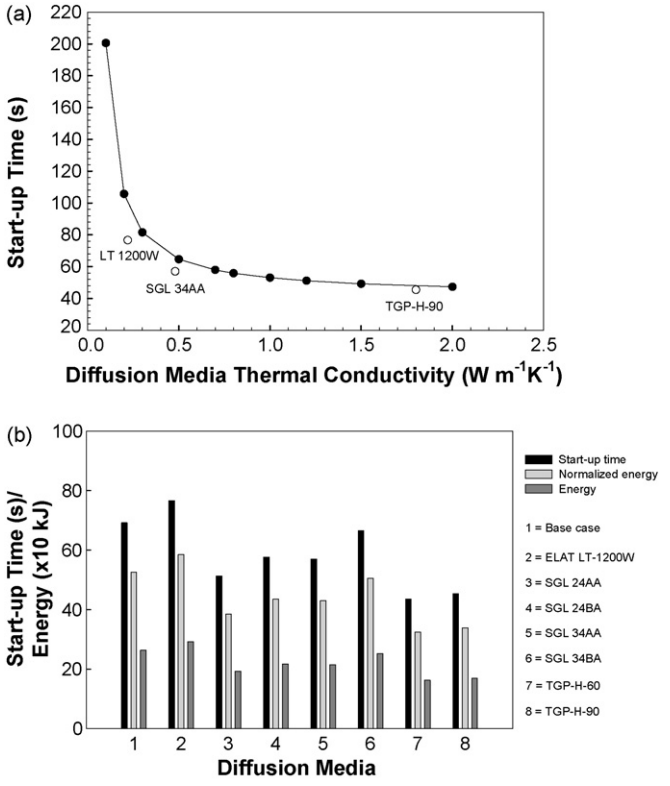

Fig. 12. (a) Effect of diffusion media thermal conductivity on the start-up time for the given thermal mass ($\rho = 450\,kg\,m^{-3}$, $C_p = 710\,J\,kg^{-1}\,K^{-1}$). (b) Start-up time and energy generation for various standard diffusion media.

are shown in Fig. 12. Although the DM are commonly ignored in the stack thermal analysis, Fig. 12a shows that the start-up time decreases from 200 to 40 s as the DM thermal conductivity increases from 0.1 to 2.0 W m^{-1} K^{-1}. Increase in DM thermal conductivity promotes the distribution of heat from the CL to the bi-polar plate, thus reducing the start-up time. It should be noted, however, that on a localized scale, lower DM thermal conductivity may also *increase* the cold-start ability of a stack, by forming an inner insulation layer, which helps locally to maintain a higher temperature at the MEA. In this case, the CL and membrane heat up faster, but other stack components will heat slowly because the heat is contained in the MEA only. Based on this analysis, a thin high thermal conducting DM with minimum thermal mass is most suitable for the rapid temperature increase and distribution across all the stack components. Fig. 12b shows the simulation results in terms of start-up time and energy requirement for various commercially available DM. For most of these commercial DM, the specific heat is not reported in the public literature. In such cases, the base case parameter is used for the cold-start simulation. Interestingly, *almost 20% reduction in start-up time* and energy requirement can be achieved by selecting the Toray carbon paper (TGP-H-90) as compared to carbon cloth from E-tek (ELAT® LT-1200 W), indicating critical role of the DM in the start-up behavior even with a generic stack design. Moreover, as *the bi-polar plate thickness is reduced in optimized stack designs compared to the baseline case tested here*, *the soft goods will become even more significant consideration for the cold-start*.

4.7. Warming mechanisms to achieve rapid start

Several external heating mechanisms, such as end plate or bi-polar plate heating [18], catalytic reaction [8,9] or passing heated fluid [12,13] can be used in the stack to reduce the start-up time. Heating of the bi-polar plates or end plates involves placing external heaters at the plate locations. In the catalytic reaction methodology, the reactant gas H_2 and O_2 is exothermally reacted to locally heat the MEA [9]. To simulate the catalytic heating, an additional heat source was specified in the membrane. Passing the heated fluid in the stack involves flow of heated coolant/anti-freeze solution or the reactant gas to the stack prior to the start-up [12,14]. These warming strategies and their effectiveness for the current stack design were analyzed and presented in the following section.

The reader should note that the appropriate external heat source is determined by the stack thermal mass and the targeted start-up time. The purpose of this analysis is to qualitatively investigate the effectiveness of various warming strategies on the start-up time. Table 4 summarizes the results for the start-up time for variations of external heat source in bi-polar plate, end plate, and due to the catalytic heating (membrane) for base conditions. The last column in Table 4 represents the ratio of percentage decrease in the start-up time and the total external heat supplied to the stack. It provides a relative metric to assess the effectiveness of adding external heat to the baseline stack. Almost 30% reduction in the start-up time was estimated from the model for 20 W external heat sources in the bi-polar plate/membrane of each cell. For the end plate heating, heating the anode side is more effective than any other heating mechanism. With a total of 200 W external heat sources, the percentage reduction in start-up time per Watt was 12.43% for anode side end plate heating. However, it was 7.7 and 7.5% for bi-polar plate and end plate (both side) external heating. The anode side end cell has the lowest temperature in the stack as already shown in Fig. 5b. External heating of the anode side end plate heats the end plate and the adjacent cells having the lowest temperature, thus it is relatively efficient means of achieving the rapid start-up, with up to 17% reduction in start-up time per Watt heat added. The start-up criterion in the model needs all location in stack to be above 0 °C. So, external heating mechanisms focused on the cooler cells (anode side end cell) will be more effective and are recommended from this study.

In all these simulation results shown in Table 4, the sensible energy flow in the stack components comprises heat sources due to ohmic and other losses (self-heating) and external heat sources. Obviously, providing external heating mechanisms decreases the start-up time substantially. But, the reduction in the start-up time should not be considered as the sole criterion

Table 4
Effect of external heating source in stack component on the start-up time (i = 1 A cm^{-2}, base condition)

Heated component	Heat source per unit component (W)	Total external heat source in the stack (W)	Start-up time (s)	% Reduction in start-up time	% Reduction per Watt ($\times 10^{-2}$)
No external heat source	0	0	69.2	–	–
Bi-polar plate	5	100	61.9	10.55	10.55
Bi-polar plate	10	200	56.3	18.64	9.32
Bi-polar plate	20	400	47.9	30.78	7.70
End plate	25	50	66.0	4.62	9.25
End plate	50	100	63.2	8.67	8.67
End plate	100	200	58.7	15.17	7.59
End plate	200	400	52.2	24.57	6.14
Anode side end plate	50	50	63.2	8.67	17.34
Anode side end plate	100	100	58.7	15.17	15.17
Anode side end plate	200	200	52.0	24.86	12.43
Membrane	5	100	61.9	10.55	10.55
Membrane	10	200	56.2	18.79	9.39
Membrane	20	400	47.9	30.78	7.70

for effectiveness of external heat source. The effective heating mechanism should contribute primarily to heat up the main stack body. Heat flow towards the end plate or the gas/coolant flow is a total waste of energy. So, to delineate the contribution of self-heating and external heating to achieve the start-up, the predicted stack temperature profile with external heaters in bi-polar plates (at 45 s), and in the end plate (at 50 s) are plotted in Figs. 13 and 14, respectively. Fig. 13a shows the stack temperature profile for the 5, 10 and 20 W heat source in the bi-polar plate of each cell. With an increase in the bi-polar plate heat source, the stack temperature rises. However, the end plate temperature remains almost same. The temperature distribution in cell 10 and the adjacent coolant plate is also shown in Fig. 13b for further justification. So, in case of bi-polar plate heating, the external heat source contributes to heat up the stack in addition to the self-heating, and thus reduced the start-up time. Similar trends were observed for the catalytic heating and are not shown here for brevity. Fig. 14 shows the stack temperature distribution for the 25, 50 and 100 W heat source in each end plate. The temperature distribution in the stack is almost same, regardless of the end plate external heat source. End plate heating contributes mainly to heat up the end plate, which is not useful, and also to the end cells. This implies that the external heat source in the end plate does not contribute substantially to reduce the start-up time. The reduction in the start-up time can be attributed to the partial heating of the end cells especially the anode side, where low temperature prevails during start-up. With the thermal isolation between end plate and current collector, the heat transfer from end plate to the end cell will be further reduced. So, heating the end plate may not be a good strategy for the rapid start-up as compared to the bi-polar plate heating, although it is much more convenient on the system level.

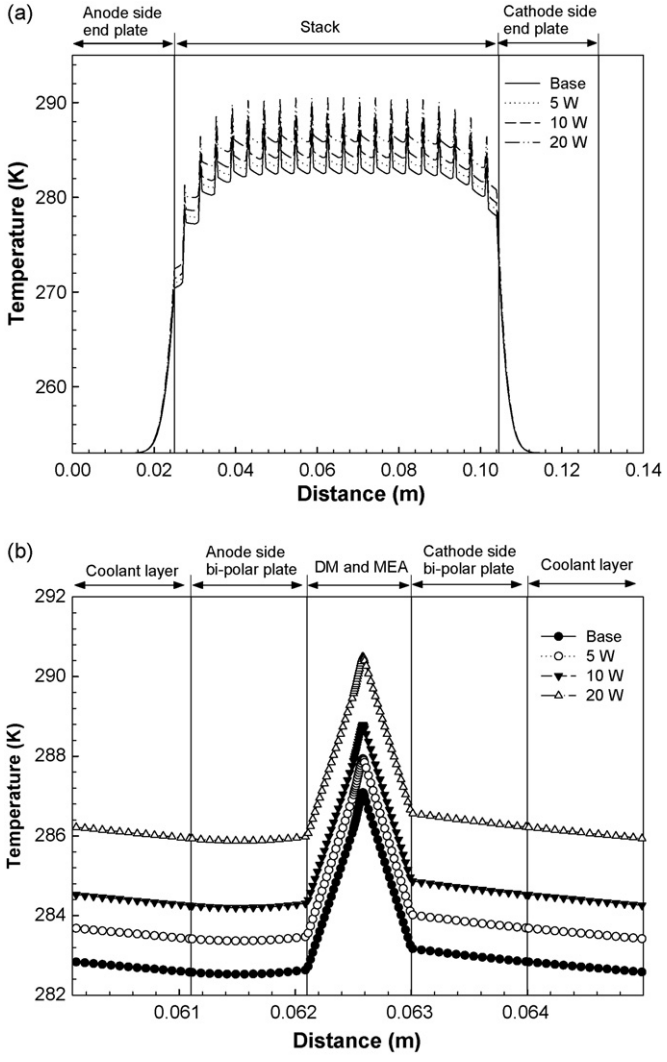

Fig. 13. (a) Stack temperature profile in 20 cell stack at the end of 45 s for additional external heat source in the bi-polar plate. (b) Temperature distribution within cell 10 at the end of 45 s.

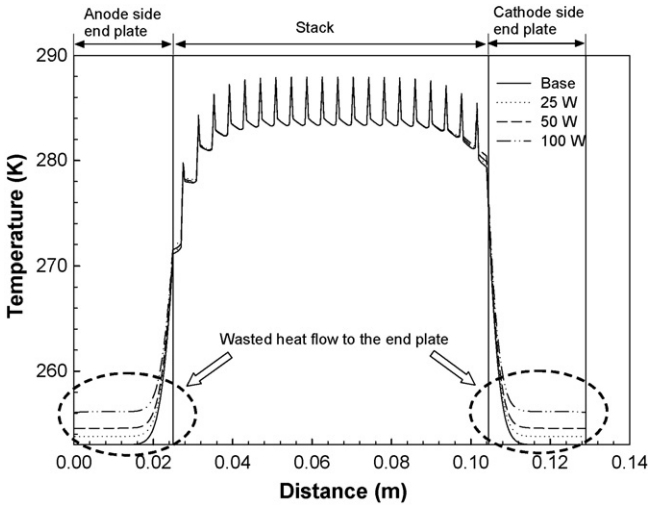

Fig. 14. Stack temperature profile in 20 cell stack at the end of 50 s for additional external heat source in each end plate.

Another heating mechanism involves passing of heated coolant or reactant gases to the stack. The effect of heated reactant gas on the start-up has already been discussed in Section 4.2. Table 5 summarizes the effect of passing the heated coolant on the stack start-up. With flow of heated coolant at 5 °C, the stack was able to start-up in less than 30 s, even at a lower current density value of 0.01 A cm^{-2}. In this scenario, nearly all the sensible and latent heat required comes from the coolant. High heat transfer rate from coolant is result of high convective heat transfer coefficient for the coolant channel. The coolant channel design should enhance the heat transfer from coolant to the

Table 5
Effect of passing the heated coolant on the start-up time (T_{amb} = −20 °C, base conditions)

Current density (A cm^{-2})	Coolant inlet temperature (°C)	Start-up time (s)	% Reduction in start-up time
Base (i = 1)	No-coolant	69.2	–
1	−5	No start-up[a]	–
1	0	No start-up[a]	–
1	2	18.2	73.70
0.1	2	No start-up[a]	–
0.1	5	25.5	63.15
0.01	5	31.4	54.62

[a] Simulations were run through 1200 s.

Table 6
Summary of model result and critical parameters for the cold-start

Parameter	Importance	Comment
Anode inlet reactant gas temperature	Moderate[a]	Heating the inlet gas (especially anode side) reduces the start-up time.
Cathode inlet reactant gas temperature	Low[a]	
Coolant inlet temperature	Critical[a]	Coolant inlet temperature > 0 °C is strongly recommended. Supplying coolant below 0 °C may retard the stack start-up, and static coolant without flow is preferred to this.
Initial ice (residual water)	Critical	Frozen residual water increases the start-up time as well as the required energy for the start-up.
Operating current density	Critical	An optimum range of operating current density exists for the cold-start.
Heat loss to the ambient (stack insulation)	Low	Stack must be insulated to minimize the heat loss to ambient.
Number of cells	Moderate	Number of cell must be above threshold value for accurate simulation of full size stack.
End plate		
Specific heat/density (ρC_p)	Moderate	Lower specific heat is better for the cold-start.
Thermal conductivity (k)	Moderate	End plate should provide thermal insulation ($k < 1\,W\,m^{-1}\,K^{-1}$). Thermal conductivity > $10\,W\,m^{-1}\,K^{-1}$ has negligible effect on start-up time.
Thickness	Moderate	Lower thickness for the end plate is recommended. Thickness higher than the threshold value has no effect on the start-up time and energy required.
Bi-polar plate		
Specific heat/density (ρC_p)	Critical	Lower thermal mass for the bi-polar plate is strongly recommended.
Thermal conductivity (k)	Low	Material with thermal conductivity > $10\,W\,m^{-1}\,K^{-1}$ is recommended.
Diffusion media		
Specific heat/density (ρC_p)	Moderate[b]	Lower thermal mass for the DM is recommended.
Thermal conductivity (k)	Moderate[b]	Higher thermal conducting DM is recommended.

[a] Gas/coolant effectiveness strongly depends on the channel convective heat transfer coefficient.
[b] These become critical as stack bi-polar plate thermal mass is minimized in an improved design.

stack body and vice versa. It is also important to note that stack was able to start-up at 1.0 A cm^{-2} without any coolant flow. But, passing the coolant below 0 °C resulted in failure to achieve the start-up condition. The reason is that coolant heats up the stack initially and reaches an equilibrium state at slightly below 0 °C. At this equilibrium temperature, coolant extracts up all the heat generated in the stack (due to the high convective loss to the coolant) and delays the start-up. Passing the coolant above 0 °C is comparatively the most effective method of external heating and achieving start-up at all current density operation.

In this work, the stack start-up results were presented using the one-dimensional thermal model. A summary of critical parameters to achieve the rapid cold-start and some conclusions are summarized in Table 6. Due to the complex stack geometry and asymmetric heating, the directional effects also have a significant impact on the start-up.

5. Conclusions

A one-dimensional thermal mathematical model was developed to predict the temperature distribution, start-up time and energy requirement, and the cold-start ability of a PEFC stack. A detailed parametric study of thermal properties of stack components and some existing materials were performed on the current stack design. The effectiveness of various warming strategies to reduce the start-up time was also investigated. Based on the model results for the given stack, the following conclusions can be made:

1. An optimum minimum number of cells are required to accurately simulate the full size stack behavior for computational and experimental testing. The minimum number of cells required in this study was found to be 20, but depends on the stack design and end plate condition.
2. For a given stack design and ambient/initial condition, an optimum range of operating current density exists to achieve the start-up condition in the shortest time, that balances heat generation with freeze-out from generated water.
3. The residual ice content contributes significantly to increase the start-up time and energy requirement, and a suitable purging methodology should be used to minimize this effect.
4. The start-up time was found to be invariant for stack bi-polar thermal conductivity greater than $10\,W\,m^{-1}\,K^{-1}$, whereas the soft goods (especially DM) thermal conductivity have a significant impact on the start-up time.
5. The bi-polar plate thermal mass has a dominating role on the start-up compared to other stack components. However, as stack designs are improved, soft goods (DM and MEA) thermal mass will become more dominant.
6. The end plates should be thermally isolated (thermal conductivity < $1\,W\,m^{-1}\,K^{-1}$) from the stack. An end plate thickness higher than the threshold value (15 mm for the base case) has no effect on the stack cold-start ability.
7. The addition of an external heat source to each bi-polar plate is useful, but complex to implement compared to heating the end plates. Of the end plate, anode side heating would be more effective to help achieve a uniform heating profile. Catalytic heating is also effective but may lead to some structural damage in MEA.
8. Pre-heating the inlet reactant gas, especially on the anode side, is effective to reduce the start-up time by 20–30%, thus improving the stack cold-start ability. Passing the coolant or anti-freeze solution at above 0 °C can be extremely effective

to achieve the rapid cold-start, even at lower current density operation.

The model developed can be used by the stack system engineers to design a specific stack with the best possible start-up strategy, given a stack specific geometry and thermal data.

Acknowledgements

This work was supported by the Advanced Technology Center, R&D Division for Hyundai Motor Company (HMC) and Kia Motors Corporation (KMC). The authors are thankful to Mr. S. Kim, Mr. J.H. Lee and Mr. J.J. Yoon for their useful comments and information for the model development.

References

[1] Q.G. Yan, H. Toghiani, Proceeding of 4th International Conference on the Fuel Cell Science, Engineering and Technology, FUELCELL2006, Irvine, CA, June 19–21, 2006, 2006.
[2] E. Cho, J. Ko, H.Y. Ha, S. Hong, K. Lee, T. Lim, I. Oh, J. Electrochem. Soc. 150 (12) (2003) A1667–A1670.
[3] S. He, M.M. Mench, J. Electrochem. Soc. 153 (9) (2006) A1724–A1731.
[4] X. Yu, B. Zhou, A. Sobiesiak, J. Power Sources 147 (2005) 184–195.
[5] J. Park, X. Li, J. Power Sources 162 (2006) 444–459.
[6] G. Maggio, V. Recupero, C. Mantegazza, J. Power Sources 62 (1996) 167–174.
[7] Y. Zong, B. Zhou, A. Sobiesiak, J. Power Sources 161 (2006) 143–159.
[8] T.F. Fuller, D.J. Wheeler, US Patent No. 6,103,410, 2000.
[9] J.A. Rock, L.B. Plant, US Patent No. 6,358,638, 2002.
[10] C.A. Reiser, US Patent No. 6,777,115, 2004.
[11] N. Matsuoka, US Patent No. 7,108,928, 2006.
[12] H.T. Couch, F. Sribnik, US Patent No. 6,773,840, 2004.
[13] G.S. Saloka, J.A. Adams, US Patent No. 6,916,566, 2005.
[14] W. Birk, US Patent No. 6,756,143, 2004.
[15] Y. Shan, S.Y. Choe, J. Power Sources 158 (2006) 274–286.
[16] Y. Shan, S.Y. Choe, S.H. Choi, J. Power Sources 165 (2007) 196–209.
[17] Y. Hishinuma, T. Chikahisa, F. Kagami, T. Ogawa, JSME Int. J. Ser. B 47 (2) (2004) 235–241.
[18] M. Sundaresan, R.M. Moore, J. Power Sources 145 (2005) 534–545.
[19] R.K. Ahluwalia, X. Wang, J. Power Sources 162 (2006) 502–512.
[20] R.K. Ahluwalia, X. Wang, R. Kumar, Fuel Cell Systems Analysis, 2006 DOE Hydrogen Program Review, Crystal City, VA, May 16–19, 2006. http://www1.eere.energy.gov/hydrogenandfuelcells/.
[21] F.P. Incropera, D.P. DeWitt, Fundamentals of Heat and Mass Transfer, 4th ed., John Wiley & Sons, 1996.
[22] M.J. Lampinen, M. Fomino, J. Electrochem. Soc. 140 (12) (1993) 3537–3546.
[23] M. Khandelwal, M.M. Mench, J. Power Sources 161 (2006) 1106–1115.
[24] S.V. Patankar, Numerical Heat Transfer and Fluid Flow, McGraw-Hill, New York, 1980.
[25] V.R. Voller, C.R. Swaminathan, Num. Heat Transfer Part B 19 (1991) 175–189.
[26] M. Khandelwal, Ph.D. Thesis Proposal, The Pennsylvania State University, 2007.
[27] A. Turhan, K. Heller, J.S. Brenizer, M.M. Mench, J. Power Sources 160 (2006) 1195–1203.
[28] Q. Yan, H. Toghiani, Y.W. Lee, K. Liang, H. Causey, J. Power Sources 160 (2006) 1242–1250.
[29] P. Argyropoulos, K. Scott, W.M. Taama, J. Power Sources 79 (1999) 169–183.
[30] Toray Carbon Paper Properties. http://www.torayca.com/index2.html.
[31] T.V. Nguyen, R.E. White, J. Electrochem. Soc. 140 (8) (1993) 2178–2186.
[32] T. Berning, D.M. Lu, N. Djilali, J. Power Sources 106 (2002) 284–294.
[33] A.J. Bard, L.R. Faulkner, Electrochemical Methods: Fundamentals and Applications, John Wiley & Sons Inc., New York, 1980.